IOPscience iopscience.iop.org

Home Search Collections Journals About Contact us My IOPscience

Intersubband absorption modulation in coupled double quantum wells by external bias

This article has been downloaded from IOPscience. Please scroll down to see the full text article.

2009 Semicond. Sci. Technol. 24 045018

(http://iopscience.iop.org/0268-1242/24/4/045018)

View the table of contents for this issue, or go to the journal homepage for more

Download details:
IP Address: 129.8.242.67
The article was downloaded on 06/07/2010 at 09:11

Please note that terms and conditions apply.

Semicond. Sci. Technol. **24** (2009) 045018 (8pp) doi:10.1088/0268-1242/24/4/045018

Intersubband absorption modulation in coupled double quantum wells by external bias

K-M Wong and D W E Allsopp

Department of Electronic and Electrical Engineering, University of Bath, Bath BA2 7AY, UK

E-mail: d.allsopp@bath.ac.uk

Received 16 December 2008, in final form 16 February 2009
Published 17 March 2009
Online at stacks.iop.org/SST/24/045018

Abstract

The scope for using intersubband absorption for electroabsorption modulation has been investigated by a detailed self-consistent solution of the coupled Schrödinger–Poisson equations. Rapid changes in intersubband absorption coefficient with electric field are predicted for modulation-doped $In_{0.53}Ga_{0.47}As/AlAs$ deep coupled quantum wells arising from a combination of Stark effect, field-induced changes in the optical matrix elements and quantum well occupancy. Extensive simulations reveal that controlling the density of electrons in the quantum wells is potentially the most robust process for prospective high-speed modulation by intersubband electroabsorption.

(Some figures in this article are in colour only in the electronic version)

1. Introduction

There is ongoing interest in exploiting intersubband absorption (ISBA) as a basis for ultrafast optical switching and modulation [1–9]. To date, most research has focused largely on applications of ISBA to all-optical switching [1–4], although its application to electroabsorption modulation has attracted recent interest [5, 6]. Whilst fast optical transitions are advantageous to both engineering applications, their requirements for effective device operation differ. In all-optical switching, rapid absorption saturation is desirable as it reduces the optical energy needed to change the switch state [4]. On the other hand, absorption saturation is unwanted in electroabsorption modulation as it reduces the modulation depth and limits the speed of the material response to voltage changes. For example, in current generation electroabsorption modulators that operate by interband absorption, the fastest absorption recovery time reported is ∼5 ps [10] at low to moderate incident optical power densities.

One alternative is to exploit ISBA. The rate of thermalization by phonon interaction after carrier excitation by ISBA depends on energy separation of the subbands in a conduction band well [11]. For an intersubband energy separation of ∼0.8 eV (corresponding to 1.55 μm wavelength telecommunication band), the relaxation time is ∼4 ps in InGaAs-based quantum wells (QWs). Whilst such a relaxation time is only a little faster than the absorption recovery time in EAMs being operated by interband absorption, thermionic emission and tunnelling will occur in parallel, offering the scope for significant improvements in the speed of the fundamental material response in devices being operated by ISBA.

Three effects contribute to electroabsorption modulation by ISBA. These are the Stark effect [5, 6], field-induced changes in the optical matrix elements and voltage control of the electron occupancy of the quantum wells. The occupancy of the ground state energy levels of a quantum system can be modulated by external bias in one of two ways: by electron transfer between coupled QWs [7, 8] or an electron reservoir [9], or by carrier depletion using the field effect as in a MODFET.

This paper describes a study of the scope for using intersubband transitions in modulation-doped coupled double quantum wells (CDQWs) as a basis for electroabsorption modulation of 1.55 μm wavelength light. The work explores the influence of the total electric field on the intersubband optical matrix elements and, in appropriately designed structures, its effect on their relative occupancy of the subbands involved in the transitions. The results show that the optimization of quantum well structures for

 © 2009 IOP Publishing Ltd Printed in the UK

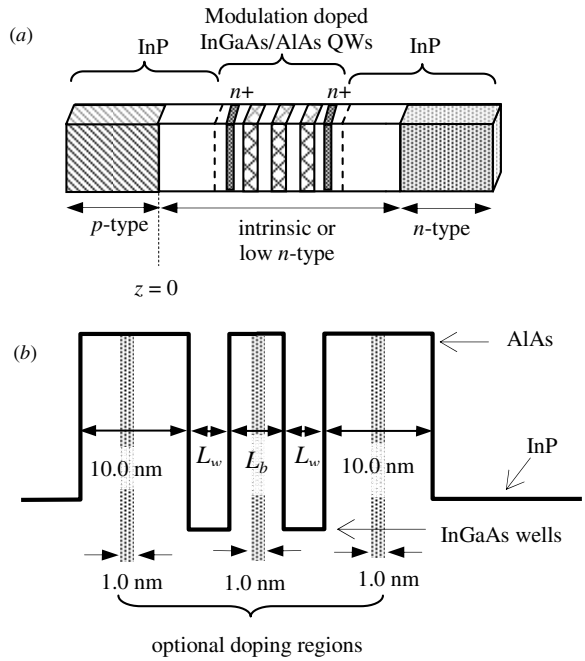

Figure 1. (*a*) Schematic of a p–i–n InP ISBA modulator with modulation-doped InGaAs/AlAs QWs. (*b*) Locations of modulation doping. The inner barrier width (L_b) is variable while the thicknesses of the outer barriers and the doping layers are kept constant in all simulations.

effective electroabsorption modulation by ISBA is potentially more complex than for devices being operated by interband transitions. It is shown that modulating the occupancy of the ground state by varying the electric field across an MQW comprising deep quantum wells via changes in the surface voltage is the most effective method of achieving absorption modulation by ISBA.

2. Model

A light modulator based on ISBA requires a high occupancy of the ground state energy levels of a quantum well (QW) or a system of coupled QWs for strong absorption and a means of inducing rapid changes in the applied electric field. Such features can be achieved by modulation doping of an MQW situated within the depletion region of a Schottky diode or a p–i–n structure, as shown schematically in figure 1.

The effect of external electric fields on ISBA in CDQWs is calculated by first obtaining a self-consistent solution of Poisson's equation and the single band effective mass Schrödinger equation [12]. The self-consistent calculations were performed for $z \geqslant 0$, where $z = 0$ defines the interface between the p and i layers (figure 1(*a*)). Thereafter the solution assumes a Schottky contact at $z = 0$. This assumption greatly simplifies the solution of the Poisson equation without compromising the simulation of the underlying device physics. Extension of the solution domain to the whole structure trivially adds a small offset voltage, to account for the space charge in the depleted p-type layer.

The self-consistent wavefunctions and subband energies and subband occupancies are then used to calculate the optical absorption coefficient via [13]

$$\alpha(\hbar\omega) = \frac{\omega\mu c e^2 m^* K_b T}{\pi\hbar^2 L n_r} \sum_{i<f} \ln\left\{\frac{1+\exp[(E_F - E_i)/K_b T]}{1+\exp[(E_F - E_f)/K_b T]}\right\} \times \langle\phi_f|z|\phi_i\rangle^2 \frac{(\Gamma/2)}{(E_f - E_i - \hbar\omega)^2 + (\Gamma/2)^2}. \quad (1)$$

In equation (1), ω is the angular frequency of the light, μ is the permeability of the QWs, m^* and n_r are the weighted effective mass and refractive index, respectively, given by [14]

$$m^* = (m_w^* L_w + m_m^* L_b)/(L_w + L_b) \quad (2)$$

$$n_r = (n_w L_w + n_b L_b)/(L_w + L_b) \quad (3)$$

where L_w is the well width, L_b is the inner barrier width in coupled QWs, n_w (n_b) is the well (barrier) refractive index, and ϕ_i, E_i and ϕ_f, E_f are respectively the envelope functions and energy minima of the initial and final subbands found from the self-consistent solution of the Poisson–Schrödinger equations. Other symbols have their usual meaning.

Both equation (1) and the Poisson–Schrödinger solver used neglect the exchange and correlation corrections arising from many body interactions [15]. At the 2DEG densities considered in this work ($<5 \times 10^{11}$ cm^{-2}), the exchange and correlation potentials will be small compared with the ~0.8 eV transition energy [16] and are neglected as being unimportant to the main features in the results.

The single band evaluation of equation (1) used here takes into account the effect of subband non-parabolicity by using an energy-dependent effect mass of the form [17]

$$m^*(E) \approx m_e(1 - \gamma E), \qquad \gamma \sim 1/E_G \quad (4)$$

where m_e is the electron effective mass at the conduction band minimum and E_G is the band gap. The effect of strain on the subband non-parabolicity factor is neglected because equation (4) is an approximation that neglects higher order terms in E.

It is assumed that the line broadening takes the form of a normalized Lorentzian function where Γ is the full-width at half-maximum (FWHM). Calculations have been performed assuming $In_{0.53}Ga_{0.47}As/AlAs$ QWs for which a value of $\Gamma \approx$ 30 meV has been reported [2, 18, 19] and is used here. Other parameter values used are $m_w^* = 0.043\ m_o$ and $m_b^* = 0.15\ m_o$ [20]; $n_w = 3.43$ and $n_b = 2.89$ [21]. With these data the model gives excellent agreement with other calculations of the intersubband transition energies of both strained InGaAs/AlAs QWs [1] and $In_{0.53}Ga_{0.47}As/In_{0.52}Al_{0.48}As$ QWs as a function of the well width [22].

3. Results and discussion

High contrast ratio optical modulation by ISBA requires parity allowed transitions at ~1.55 μm wavelength. This condition is met by the intersubband transition from level E_1 to level E_2 (denoted by E_{if} where i is the initial state and f is the final state) in $In_{0.53}Ga_{0.47}As/AlAs$ QWs grown on InP for well widths of 2.2 nm. The feasibility of growing such narrow strongly coupled double QWs (CDQWs) is well established [23, 24]. Further, narrow single QWs and CDQWs have been shown to

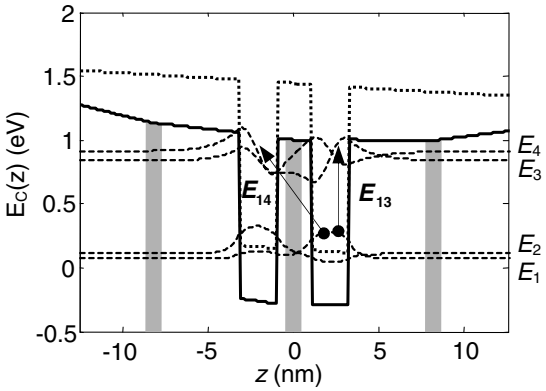

Figure 2. Calculated conduction band profiles of a modulation-doped InGaAs/AlAs and an undoped CDQW structure comprising two 2.2 nm wide wells separated by a 2 nm wide inner barrier. Also shown are the envelope function of the four subbands and the definition of spatially direct transitions in the same well and the spatially indirect transitions between adjacent wells.

be effective for achieving fast optical response intersubband transitions in practical device structures [1–4, 18].

In such narrow QWs, a strong field dependence of the optical matrix elements is not expected, as the wavefunction overlap remains significant for all but the highest electric field. The use of CDQWs overcomes this problem, as wavefunctions readily localize into one or other of the wells when an electric field is applied. Figure 2 shows the calculated energy band profile (heavy solid line) and wavefunctions (dashed lines) of a biased modulation-doped CDQW. The donors ($N_D = 5 \times 10^{17}$ cm^{-3}) are located in two 1 nm wide layers centred at a distance 5 nm into the outer barriers. Also shown is the band profile of the same CDQW but without modulation doping (light solid line). In all the structures considered, the distributions of the wavefunctions and hence the optical matrix elements are very sensitive to the local band bending which is determined by the positioning of any modulation doping and the surface potential. Since the absorption strength depends on both the optical matrix element and occupancy of the two lower energy levels in the CDQW, a consistent baseline for defining the bias point of the different QW structures considered is required. For this purpose the integrated average of the electric field over the solution domain is used to describe the bias point. The conduction band profiles shown in figure 2 are for an average applied field of $F_{\rm av} = -10$ V μm^{-1} but show their variation with position.

The calculated wavefunctions for the four confined electron states of the CDQW are also shown in figure 2. The amplitudes of the wavefunctions at the right edge of the graph coincide approximately with the energy levels of the bottoms of the subbands within the wells. Intersubband transitions from the E_1 and E_2 ground states of the CDQW structure can be classified into two groups: spatially direct transitions within the same well (E_{13} and E_{24}) and spatially indirect transitions between adjacent wells (E_{14} and E_{23}). The arrows in figure 2 indicate the E_{13} spatially direct and the E_{14} spatially indirect transitions. As will be seen, the effect of an externally applied electric field on spatially direct transitions differs from that on spatially indirect transitions. Whilst both effects create opportunities for achieving absorption modulation, these are not usually complementary.

In order to understand the relative roles of the matrix elements and the subband occupancy in the modulation of ISBA, an initial set of simulations were performed for an CDQW with a uniform low n-type doping background level of 1×10^{15} donors cm^{-3} equivalent to residual unintentional doping, to minimize the effects of the band bending associated with the ionized donors in any modulation-doped layers. The CDQW comprised two 2.2 nm $In_{0.53}Ga_{0.47}As$ wells separated by a 2 nm wide AlAs inner barrier and AlAs outer wells. Figure 3(*a*) shows the calculated effect of an applied electric field on the E_{13}, E_{14}, E_{23} and E_{24} intersubband transitions. The other panels of figure 3 show the effect of the applied field on (*b*) the peak contribution each transition makes to the intersubband absorption band of the same CDQW structure, (*c*) the matrix elements of the E_{13}, E_{14}, E_{23} and E_{24} intersubband transitions and (*d*) the occupancy ratios of the subbands involved in each transition.

Figure 3(*b*) shows that the spatially indirect E_{14} and E_{23} transitions dominate the intersubband absorption band for electric field strengths $0 < |F_{\rm av}| < 8$ V μm^{-1}. E_{14} absorption is the stronger, reflecting the higher carrier occupancy of the E_1 subband. Over this field range the maximum absorption of these two transitions varies by a factor $\sim 1 \times 10^4$, reflecting the same order of magnitude change in their electron occupancy ratio (figure 3(*d*)). On the other hand, the optical matrix elements of the E_{14} and E_{23} transitions vary monotonically by only a factor $\sim$4 over the whole field range considered ($0 < |F_{\rm av}| < 15$ V μm^{-1}).

Over the same field range, the optical matrix element of the spatially direct E_{13} transition, $\langle\psi_3|z|\psi_1\rangle$, increases, rapidly so for $|F_{\rm av}| < \sim 2$ V μm^{-1}, as the parity selection rule breaks down (figure 3(*c*)). The spatially indirect E_{14} transition still dominates the absorption band for field strengths up to $|F_{\rm av}| \sim 8$ V μm^{-1}. In fact, for $|F_{\rm av}| > \sim 5$ V μm^{-1}, the electric field dependence of the absorption strength of all the intersubband transitions closely follows the almost exponential change in the occupancy ratio with field. The only impact of the variations in the optical matrix elements is the change in relative strengths of the contributions of the E_{13} and E_{14} transitions to the absorption spectrum occurring at $|F_{\rm av}| \sim 8$ V μm^{-1}. This arises from the simultaneous slow increase in $\langle\psi_3|z|\psi_1\rangle$ and decrease in $\langle\psi_4|z|\psi_1\rangle$ with $F_{\rm av}$. Overall, the absolute change in the strength of the total intersubband absorption is still governed by field-induced variations in the occupancy ratio, i.e. by carrier depletion.

The changes in the transition energies with electric field have only a weak effect on the occupancy ratio, as again this is dominated by the occupancy of the lowest energy subbands. This is seen more clearly in the results that follow.

Rapid changes in the optical matrix elements of the spatially direct and indirect intersubband transitions in stepped QWs have been reported and proposed as a basis for optical modulation [5]. Similar rapid changes in the optical matrix elements of the direct transitions E_{13} and E_{24} in a CDQW also offer a very sensitive means of modulating intersubband

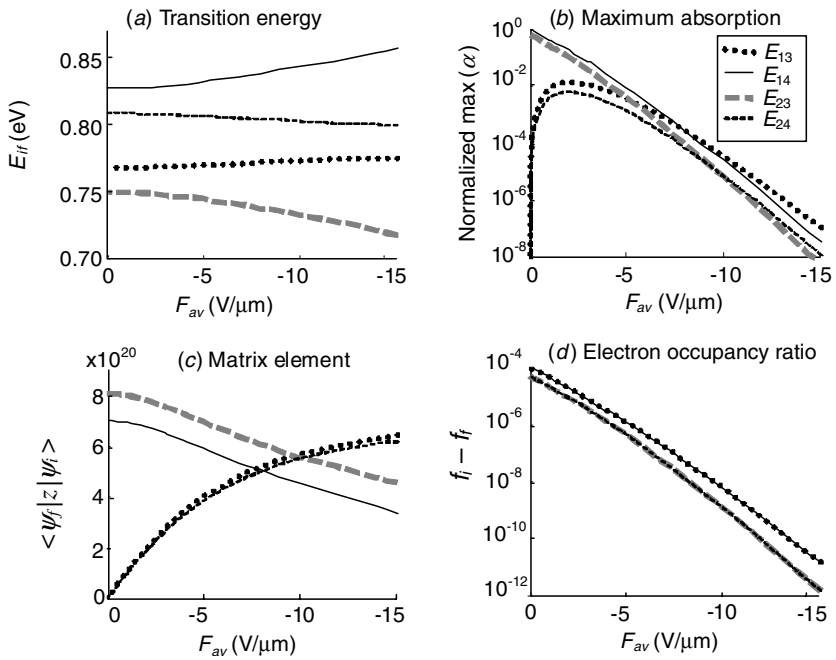

Figure 3. Electric field dependence of (*a*) transition energy, (*b*) normalized maximum absorption, (*c*) optical matrix element and (*d*) electron occupancy ratio in an undoped CDQW comprising two 2.2 nm $In_{0.53}Ga_{0.47}As$ wells separated by a 2 nm wide AlAs inner barrier. The inset in (*b*) relating the line type to the identified intersubband transition also applies to panels (*a*), (*c*) and (*d*).

absorption. However, in the presence of the high carrier densities essential to strong ISBA the field distribution across an MQW will be non-uniform. Consequently, biasing each well to the field region in which the absorption modulation is monotonic with applied bias will be difficult, if not impossible, to achieve.

On the other hand, using the absorption bands associated with the indirect E_{23} or E_{14} transitions and controlling the 2DEG density in a modulation-doped structure by carrier depletion via a Schottky or p-type contact offers a robust method of modulating ISBA. Figure 3(*b*) shows that small changes in the applied field across an MQW will merely shift the operating point of each CDQW along a monotonically varying characteristic allowing additive absorption contributions for each period added to the MQW.

Exploiting the indirect E_{23} or E_{14} transitions has two other advantages. First, the doping density can be increased to enhance simultaneously the occupancy of the ground and the off-state absorption. Second, modulation doping can be incorporated strategically in one or more of the barriers of the CDQW, as shown in figure 1(*b*), to adjust the built-in field across an MQW and hence the operating point of the device.

Figure 4 shows the impact of such strategic modulation doping on the absorption-voltage characteristic of a device operating at a wavelength at which the ISBA is dominated by the E_{14} transition. The device is assumed to have the epitaxial structure shown in figure 1 with a Schottky contact of barrier height of 0.5 eV on the left and an n-type InP layer on the right. The modulation doping was added in one or more of the locations indicated. In the simulations, the AlAs barrier on the left of the double well structure is always assumed to be that nearest the Schottky contact. In all cases the modulation-doped region was 1 nm wide containing a donor density of

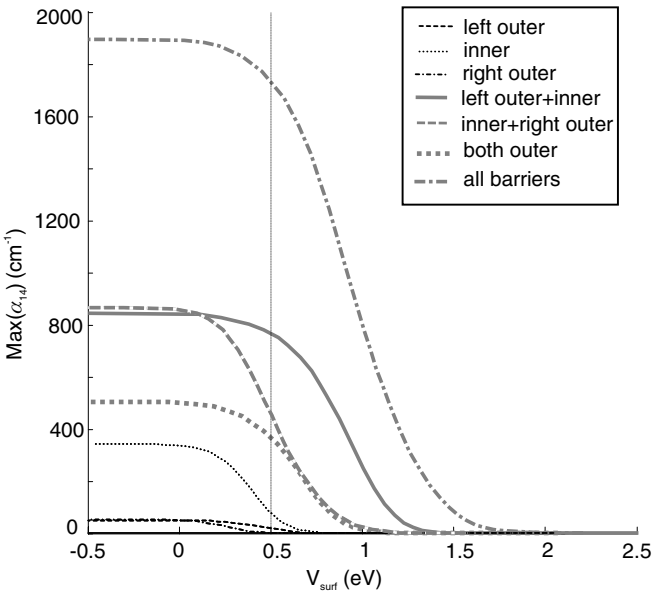

Figure 4. Effect of doping location on the dependence of the maximum absorption coefficient of the E_1–E_4 transition on surface voltage. All modulation doping layers were 1.0 nm wide and contained 1×10^{18} donors cm^{-3}.

1×10^{18} donors cm^{-3}. When sited in the inner barrier, the doped layer is positioned symmetrically between the wells. When sited in the left or right outer barriers, the doped layer is positioned 5 nm from the outer edge of the QW. The vertical dashed line indicates the value where the surface potential, V_{surf}, equals the assumed contact potential of 0.5 eV.

The results in figure 4 show that the peak absorption does not increase linearly with the total number of donors,

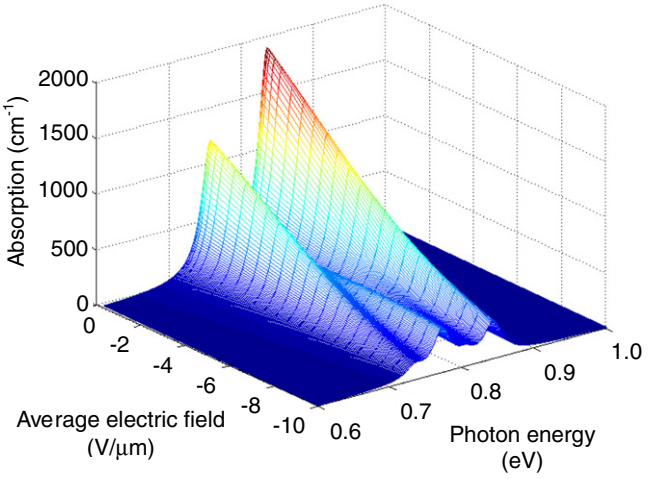

Figure 5. Variation of absorption coefficient with photon energy and electric field for coupled 2.2 nm wide $In_{0.53}Ga_{0.47}As/AlAs$ QWs, with $L_B = 2$ nm, modulation-doped with 1×10^{18} donors cm^{-3} in 1 nm wide layers in the inner and both outer barriers. (Intensity colour code: quantitative levels can be read from the vertical axis with red = high intensity, blue = low intensity.)

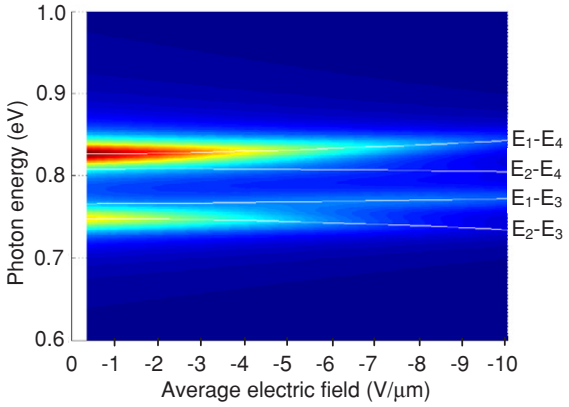

Figure 6. Electric field dependence of the intersubband transition energies of the same modulation-doped CDQW as in figure 5 with a colour map of the absorption strength superimposed. (Intensity colour code: as in figure 5.)

but depends on the position of the modulation-doped regions. This is because of the variation in the screening effect of the ionized donors on the biased contact, in this case an assumed Schottky contact on the left of the solution domain. If only one barrier is modulation doped, locating the donors in the inner barrier between the wells has the greatest effect by pulling the two wells downward in energy towards the Fermi level, to increase the occupancy of level E_1 (see the light dotted line in figure 4 and the effect of doped layers on band bending in figure 2). This increases the intersubband absorption coefficient for transition E_{14}. Adding doping to only one of the outer barriers results in almost the same increase in the peak absorption, but the threshold voltage for no absorption changes because positioning the donors in the left-hand barrier has a stronger screening effect on the biased contact compared with modulation doping the right-hand outer barrier. The highest peak absorption occurs when doped layers are inserted in all the barriers. With a semi-insulating substrate (not considered here), locating the donors in the inner barrier, or even in the wells, will be most effective in increasing the maximum absorption strength, because the conduction band edge will be raised away from the Fermi level.

In the structures modelled, the maximum sheet carrier density in the CDQW considered is only 3×10^{11} cm^{-2}, a moderate doping level compared with a HEMT. Yet this is sufficient to yield a maximum IBSA strength of $\sim$1900 cm^{-1} for a single period CDQW when the modulation doping is applied to all three barriers (a dot-dash grey line in figure 4).

Figure 5 shows the evolution with the electric field of the whole intersubband absorption spectrum of a modulation-doped strongly coupled CDQW designed to operate at $\sim$1.55 μm wavelength. The CDQW comprises two $In_{0.53}Ga_{0.47}As/AlAs$ deep QWs of width $L_w = 2.2$ nm separated by a barrier of width $L_b = 2.0$ nm, with modulation doping of $N_D = 1 \times 10^{18}$ donors cm^{-3} in 1 nm wide regions in all AlAs barriers, as indicated in figure 1(*b*).

The overall shape of the absorption band is complex, reflecting the differences in the electric field dependence of the optical matrix elements of the direct (E_{13}, E_{24}) and indirect (E_{23}, E_{14}) intersubband transitions in a CDQW shown in figure 3(*b*). At a low applied field, the contributions from the indirect transitions E_{14} at $\sim$0.83 eV and E_{23} at $\sim$0.75 eV dominate the absorption band, owing to the combination of large optical matrix elements and high electron occupancy factors of the E_1 and E_2 states. The absorption strength of both these bands decreases monotonically with increasing applied electric field, to produce the type of rapidly varying peak absorption–voltage characteristic shown in figure 4.

On the other hand, the contributions from transitions E_{13} and E_{24} are negligibly small at low applied electric fields but grow rapidly with increasing field strength. Despite the apparent absorption strength of the transition E_{13} when $|F_{av}| \geqslant 10$ V μm^{-1}, it in fact has only a small effect on the overall absorption modulation due to the extended Lorentzian tail of the line broadening effect of the E_{14} and E_{23} transitions. At best, the maximum absorption strength of the E_{13} transition is only $\sim$450 cm^{-1} (at $|F_{av}| = 8$ V μm^{-1}) compared with $\sim$2000 cm^{-1} for the E_{14} transition (at $|F_{av}| = 0$).

Figure 6 reveals the contribution of the Stark shift of the absorption peaks to the absorption modulation at fixed wavelength in this modulation-doped structure. The energy of the direct transitions, E_{13} and E_{24}, varies only slightly with field, whereas the energies of the indirect transitions vary significantly with the strength of the applied electric field. E_{14} undergoes a blue shift of $\sim$200 meV whilst E_{23} undergoes a red shift of the same size as $|F_{av}|$ varies from 0 to 10 V μm^{-1}. In both cases, the change in transition energy with applied field strength contributes to the rapid monotonic absorption change that occurs for photon energies lying within $\sim$50 meV of the E_{14} and E_{23} transition peaks.

The properties of the basic CDQW will depend on the width of the barrier, L_b, between the two wells. This will alter the strength of the coupling between the two QWs, influencing the Stark shift and the field dependence of the intersubband optical matrix elements. Figure 7 shows the variation of (*a*) the

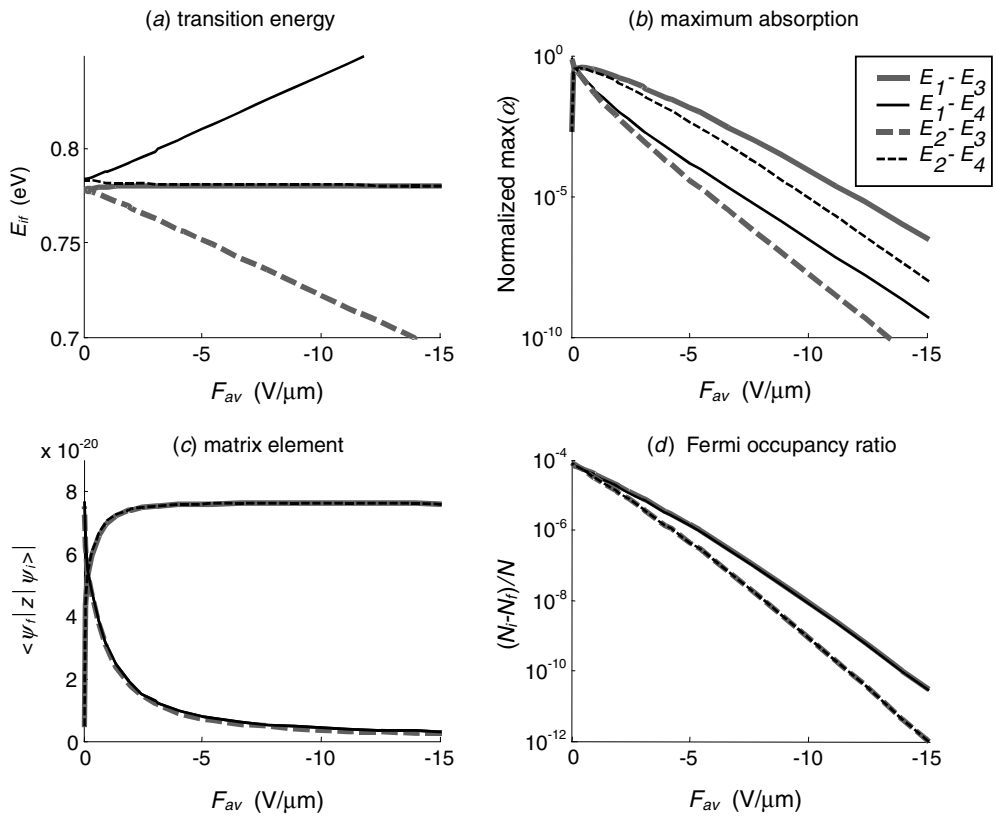

Figure 7. Electric field dependence on (*a*) transition energy, (*b*) maximum absorption, (*c*) optical matrix element and (*d*) electron occupancy ratio in an undoped CDQW comprising two 2.2 nm $In_{0.53}Ga_{0.47}As$ wells separated by a 5 nm wide AlAs inner barrier that results in only weak coupling of the quantum wells. The inset in (*b*) relating the line type to the identified intersubband transition also applies to panels (*a*), (*c*) and (*d*).

transition energy, (*b*) the maximum absorption strength, (*c*) the absolute value of the optical matrix element and (*d*) the Fermi occupancy ratio of the same basic CDQW as that considered in figure 3 but with the inner barrier increased from 2 nm to 5 nm. Again, the structure is undoped to avoid complications arising from the spatial variations in the built-in field associated with the incorporation of modulation doping.

Weakening the coupling between the wells has a major effect on the intersubband behaviour. The Stark shifts (figure 7(*a*)) of the indirect E_{14} and E_{23} transitions, respectively to blue and red, become stronger, whilst the direct E_{13} and E_{24} transitions become degenerate and almost invariant with field strength (cf figure 3(*a*)). Outside a very narrow, in practice inaccessible, field range close to zero, the absorption strength of all four intersubband transitions now decreases with increasing average electric field strength (figure 7(*b*)). This behaviour is governed by the field dependence of the Fermi occupancy ratio of the transitions involved (figure 7(*d*)), as the field-induced changes in the optical matrix elements are much smaller (figure 7(*c*)).

Despite the strong Stark shift of the spatially indirect E_{14} and E_{23} transitions giving rise to a more rapid reduction in the absorption coefficient of these features, in absolute terms the absorption strengths of the spatially direct E_{13} and E_{24} transitions are much greater over the whole electric field range. As figure 7(*d*) shows, the absorption modulation is governed by the change in occupancy of the E_{13} transition. Further, the near degeneracy of the E_{13} and E_{24} transitions means their absorption peaks almost coincide in energy, making their contributions additive to reinforce their dominant role in electroabsorption.

Figure 8 shows the dependence of absorption coefficient on photon energy and electric field for modulation-doped coupled 2.2 nm wide $In_{0.53}Ga_{0.47}As/AlAs$ QWs, but with L_B increased to 5 nm. The modulation doping comprised 1×10^{18} donors cm^{-3} in 1 nm wide layers arranged in both outer barriers and the inner barrier in a manner illustrated in figure 1(*b*).

The absorption spectrum now contains only a single peak centred on a photon energy of ∼0.78 eV. This derives from vertical transitions E_{13} and E_{24} which are all but degenerate owing to the rapid localization of the wavefunctions to the individual wells. The strength of the absorption peak declines rapidly and monotonically with hardly any Stark shift as the applied electric field increases. As such, the behaviour is very different from that of the strongly coupled well case (figure 5) and resembles that of a single QW.

The monotonic variation of the absorption band with applied field strength arising from the change in occupancy of the E_1 and E_2 energy levels is advantageous for optical modulation. In a practical device, a modulation-doped MQW will be needed to achieve sufficient signal modulation depth without excessive waveguide length and hence large capacitance. With modulation doping the 2DEGs in each

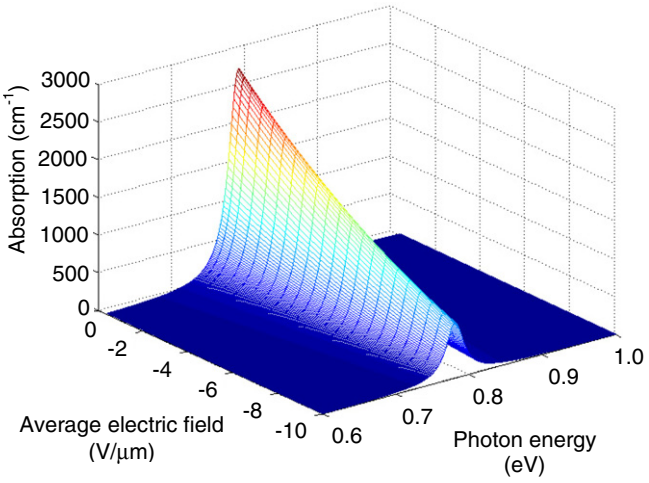

Figure 8. Variation of absorption coefficient with photon energy and electric field for weakly coupled 2.2 nm wide $In_{0.53}Ga_{0.47}As/AlAs$ QWs, with $L_B = 5$ nm, modulation-doped with 1×10^{18} donors cm^{-3} in 1 nm wide layers in the inner and both outer barriers. (Intensity colour code: as in figure 5.)

of wells will deplete in sequence with increasing bias. Consequently, each well will be at a different bias point. The unchanging shape of the absorption band of a single CDQW with electric field means that the absorption band of the MQW will be the simple addition of similarly shaped absorption bands if somewhat broadened by well width fluctuations in practice. This will enable straightforward optimization of an ISBA modulator based on such weakly coupled modulation-doped CDQW, or even single QWs.

4. Summary

The scope for achieving absorption modulation of 1.55 μm wavelength light by ISBA in a range of deep modulation-doped $In_{0.53}Ga_{0.47}As/AlAs$ strongly and weakly coupled QWs has been demonstrated by detailed simulation. The most effective means of achieving absorption modulation for both strongly and weakly coupled CDQWs is shown to be field effect, namely electric-field-induced changes in the occupancy of the ground state energy levels in the CDQWs. The absorption coefficient decreases rapidly and monotonically as the wells are depleted of electrons by the electric field. The simple shape of the intersubband absorption spectrum of weakly coupled CDQW is potentially more advantageous for realizing a practical modulator being operated by ISBA since the absence of a strong Stark shift and dominance of the occupancy factor in the field dependence of the absorption enable straightforward design optimization.

References

[1] Hurayama Y, Smet J H, Peng L-H, Fonstad C G and Ippen E P 1994 Feasibility of 1.55 μm intersubband photonic devices using InGaAs/AlAs pseudomorphic quantum well structures *Japan. J. Appl. Phys.* **33** 890

[2] Yoshida H, Mozume T, Neogi A and Wada O 1999 Ultrafast all-optical switching at 1.3 μm/1.55 μm using novel InGaAs/AlAsSb/InP coupled double quantum well structure for intersubband transitions *Electron. Lett.* **35** 1103

[3] Akiyama T, Georgiev N, Mozume T, Yoshida H, Gopal A V and Wada O 2002 1.55 μm picosecond all-optical switching by using intersubband absorption in InGaAs-AlAs-AlAsSb coupled quantum wells *IEEE Photon. Technol. Lett.* **14** 495

[4] Gopal A V, Simoyama T, Yoshida H, Kasai J, Mozume T and Ishikawa H 2003 Intersubband absorption saturation in InGaAs-AlAs-AlAsSb coupled quantum wells *IEEE J. Quantum Electron.* **39** 1356

[5] Holmström P 2001 High-speed mid-IR modulator using Stark shift in step quantum wells *IEEE J. Quantum Electron.* **37** 1273

[6] Liu H C, Song C Y, SpringThorpe A J and Aers G C 2003 Infrared quantum well intersubband modulator *Electron. Lett.* **29** 1149

[7] Duboz J Y, Berger V, Laurent N, Adam D and Nagle J 1997 Grating coupled infrared transitions at normal incidence based on intersubband transitions *Appl. Phys. Lett.* **70** 1569

[8] Kheirodin N *et al* 2008 Electrooptical modulator at telecommunication wavelengths based on GaN-AlN coupled quantum wells *IEEE Photon. Technol. Lett.* **20** 724

[9] Baumann E, Giorgetta F, Hofstetter D, Leconte S, Guillot F, Bellet-Amalric E and Monroy E 2006 *Appl. Phys. Lett.* **89** 101121

[10] El Dahdah N, Aubin G, Harmand J-C, Ramdane A, Shen A, Devaux F, Garreau A and Benkelfat B-E 2004 Ultrafast InGaAs/InGaAlAs multiple quantum well electro-absorption modulator for wavelength conversion at high bit rates *Appl. Phys. Lett.* **84** 4268

[11] Asano T, Noda S and Tomoda K 1999 Pump and probe measurement of intersubband relaxation time in short wavelength intersubband transition *Appl. Phys. Lett.* **74** 1418

[12] Wilson S P, Morton C G and Allsopp D W E 1992 Application of an efficient algorithm for solving the one band effective mass equation self-consistently in the modelling of some low dimensional structure devices *Int. J. Numer. Modelling* **5** 23

[13] Ahn D and Chuang S L 1987 Intersubband optical absorption in a quantum well with an applied electric field *Phys. Rev.* B **35** 4149

[14] Nojima S 1990 Intraband optical absorption in semiconductor superlattices *Phys. Rev.* B **41** 10214

[15] Kim K Y, Lee B and Lee C 1999 Modelling of intersubband and free carrier absorption coefficients in heavily doped conduction band quantum well structures *IEEE J. Quantum Electron.* **35** 1491

[16] Carline R T and Allsopp D W E 1991 A simplified self-consistent model of charge control in quasi-square quantum well HFETs *Semicond. Sci. Technol.* **6** 1151

[17] Nelson D F, Miller R C and Kleinman D A 1987 Band non-parabolicity effects in semiconductor quantum wells *Phys. Rev.* B **35** 7770

[18] Neogi A, Mozume T, Yoshida H and Wada O 1999 Intersubband transitions at 1.3 and 1.55 μm in a novel coupled InGaAs/AlAsSb double-quantum well structure *IEEE Photon. Technol. Lett.* **11** 632

[19] Ghislotti G, Riedo E, Ielmini D and Martinelli M 1999 Intersubband relaxation time for $In_xGa_{1-x}As/AlAs$ quantum wells with large transition energy *Appl. Phys. Lett.* **75** 3626

[20] Vurgaftman I, Meyer J R and Ram-Mohan L R 2001 Band parameters for III–V compound semiconductors and their alloys *J. Appl. Phys.* **89** 5815

[21] Bhattacharya P 1993 Properties of III-V quantum wells and superlattices (Stevenage, UK: INSPEC Institution of Electrical Engineers)

[22] Asai H and Kawamura Y 1991 Intersubband absorption in $In_{0.53}Ga_{0.47}As/In_{0.52}Al_{0.48}As$ multiple quantum wells *Phys. Rev.* B **43** 4748

[23] Bhatnagar A, Chen X, Allsopp D W E, Earnshaw M P and Batty W 2000 Electrorefraction associated with Wannier-Stark localisation in strongly coupled three quantum well structures *IEEE J. Quantum Electron.* **36** 702

[24] Earnshaw M P and Allsopp D W E 2001 Electro-optic effects in GaAs/AlGaAs narrow coupled quantum wells *IEEE J. Quantum Electron.* **37** 897